

## Strong Intermolecular Polarization to Boost Polysulfides Conversion Kinetics for High Performance Lithium-Sulfur Battery

Yin Hu <sup>a,b,1</sup>, Anjun Hu <sup>b,1</sup>, Jianwei Wang <sup>a,1</sup>, Xiaobin Niu <sup>a,\*</sup>, Mingjie Zhou <sup>b</sup>, Wei Chen <sup>b</sup>, Tianyu Lei <sup>b</sup>, Jianwen Huang <sup>b</sup>, Yaoyao Li <sup>b</sup>, Lanxin Xue <sup>b</sup>, Yuxin Fan <sup>b</sup>, Xianfu Wang <sup>b,\*</sup>, Jie Xiong <sup>b,\*</sup>

<sup>a</sup> *School of Materials and Energy, University of Electronic Science and Technology of China, Chengdu 610054, China*

<sup>b</sup> *State Key Laboratory of Electronic Thin Films and Integrated Devices, University of Electronic Science and Technology of China, Chengdu 610054, China*

\* Corresponding Author: [jiexiong@uestc.edu.cn](mailto:jiexiong@uestc.edu.cn)

<sup>1</sup> Yin Hu, Anjun Hu and Jianwei Wang contribute equally to this work.

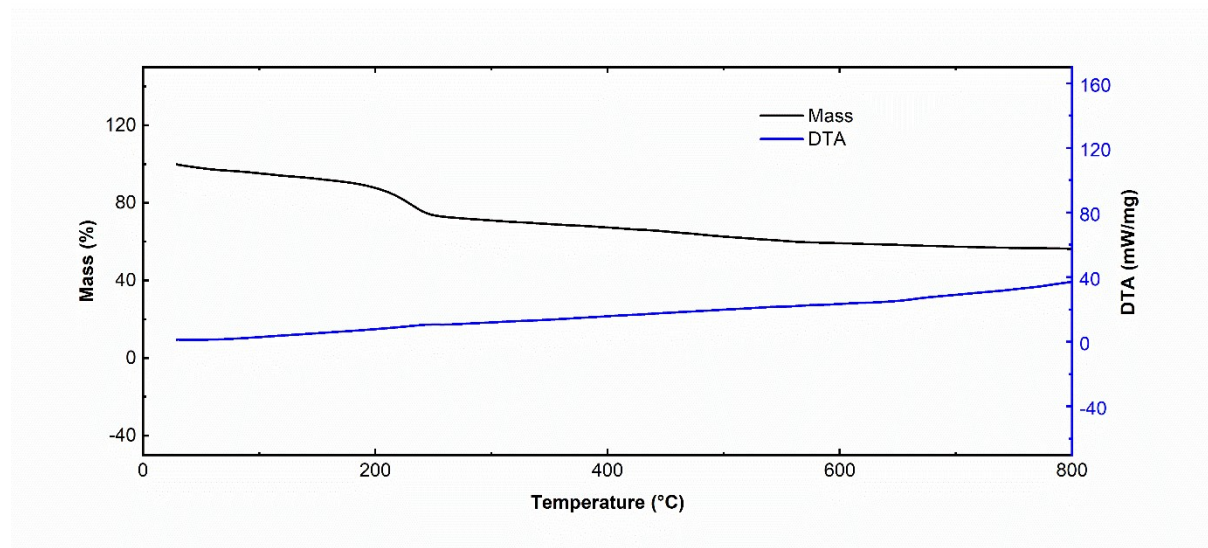


**Fig. S1** TGA curve of CIS0 under N<sub>2</sub>.

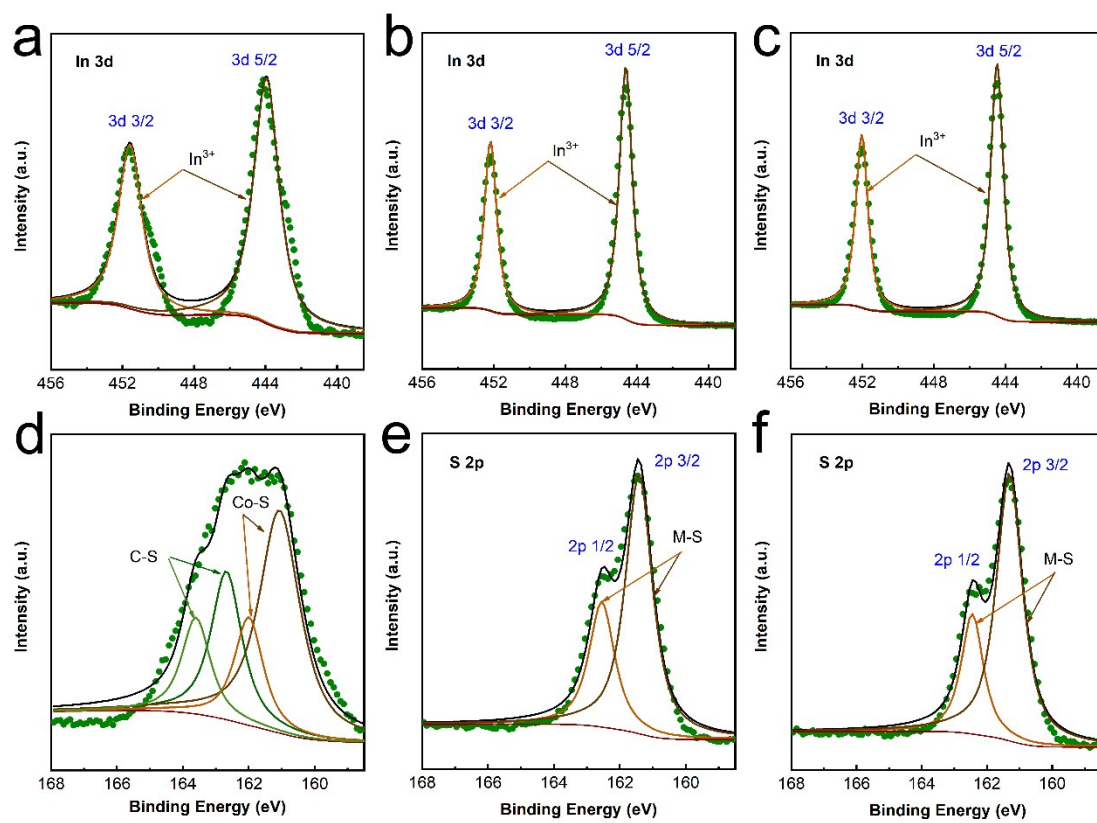


**Fig. S2** XPS In 3d (a-c) and S2p (d-e) spectra of a,d) CIS0, b,e) CIS400 and c,e) CIS600, respectively.

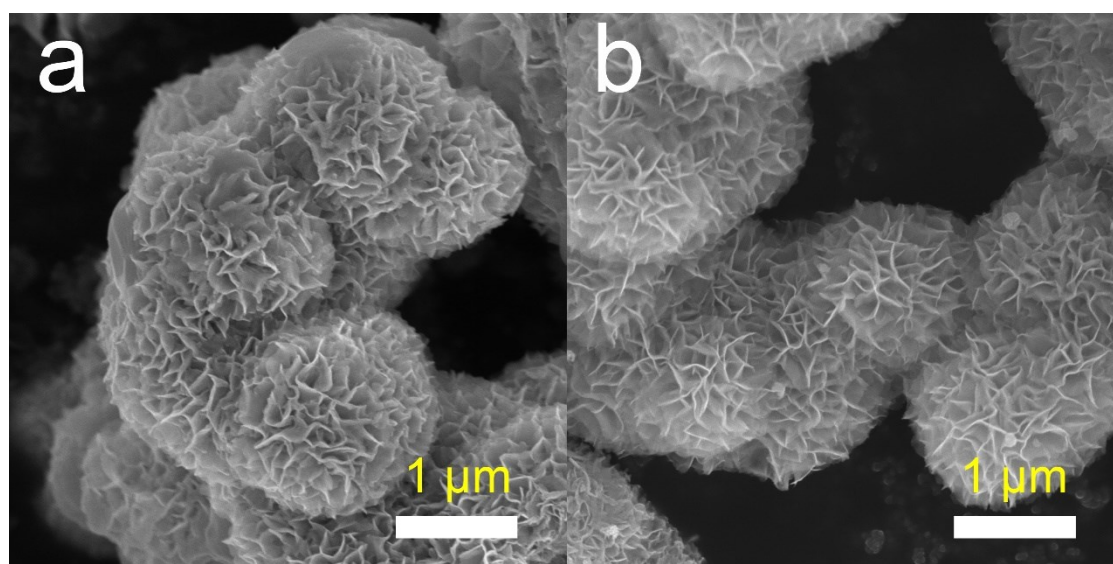


**Fig. S3** SEM images of a) CIS400 and b) CIS0.

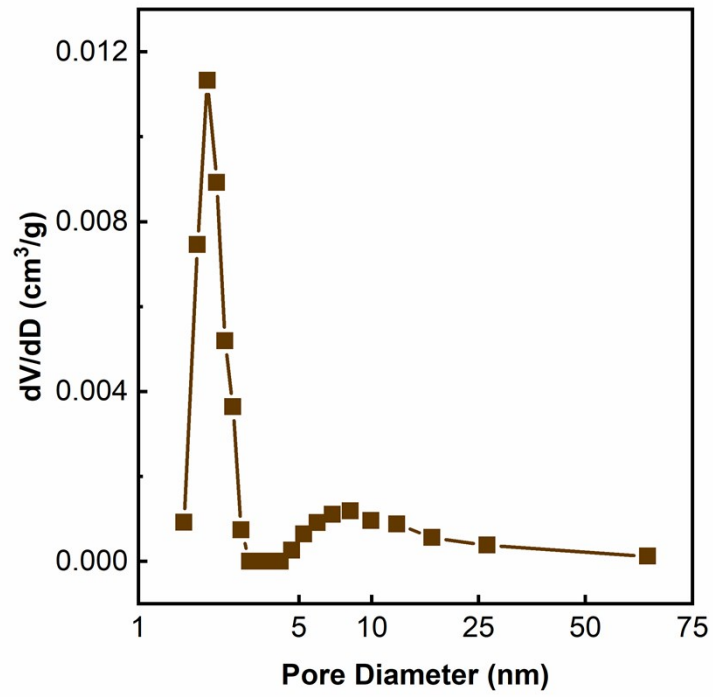


**Fig. S4** Pore distribution curve of CIS0.

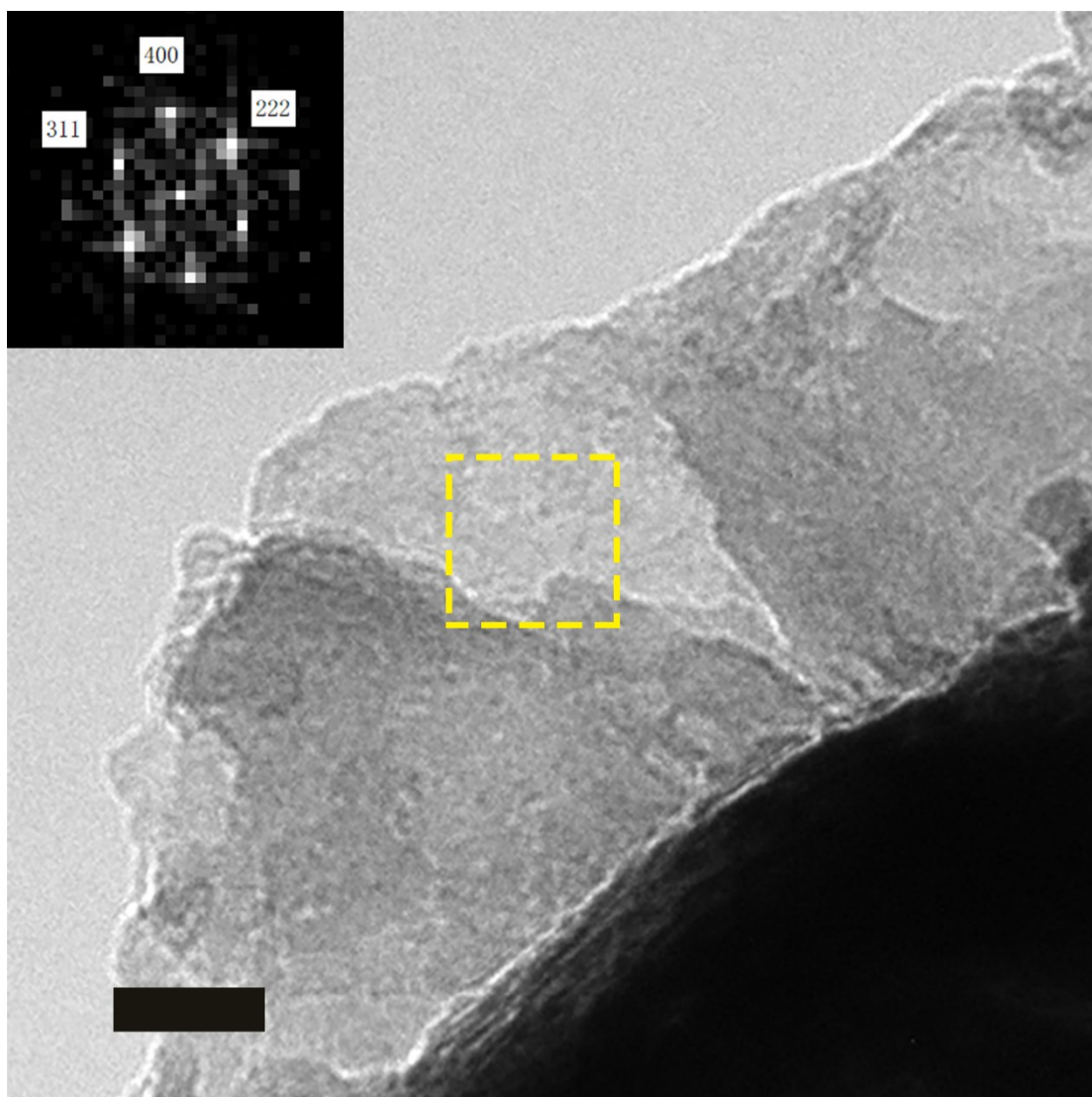


**Fig. S5** TEM image locating at the edge of CIS600. Inset is the corresponding FFT pattern. Scale bar is 20 nm.

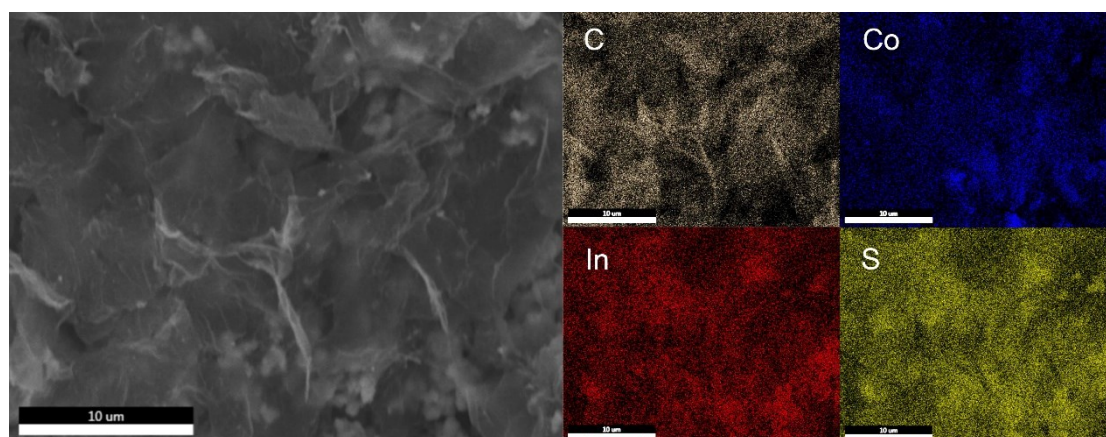




**Fig. S6** EDS mapping of the selected area for the CIS600/RGO coated separator.

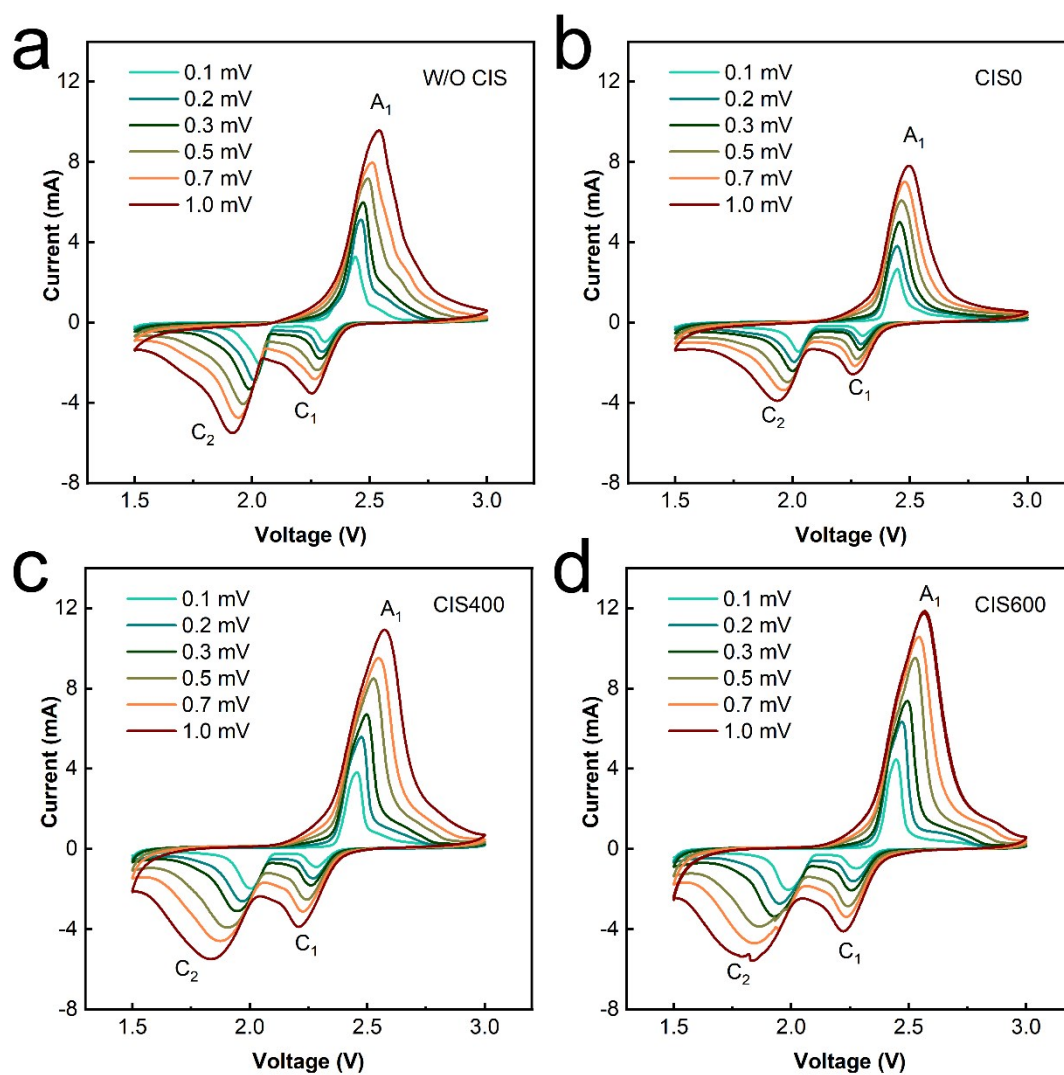


**Fig. S7** CV measurements performed at different scan rates for the Li-S batteries a) without CIS, with b) CIS0, c) CIS400 and d) CIS 600.

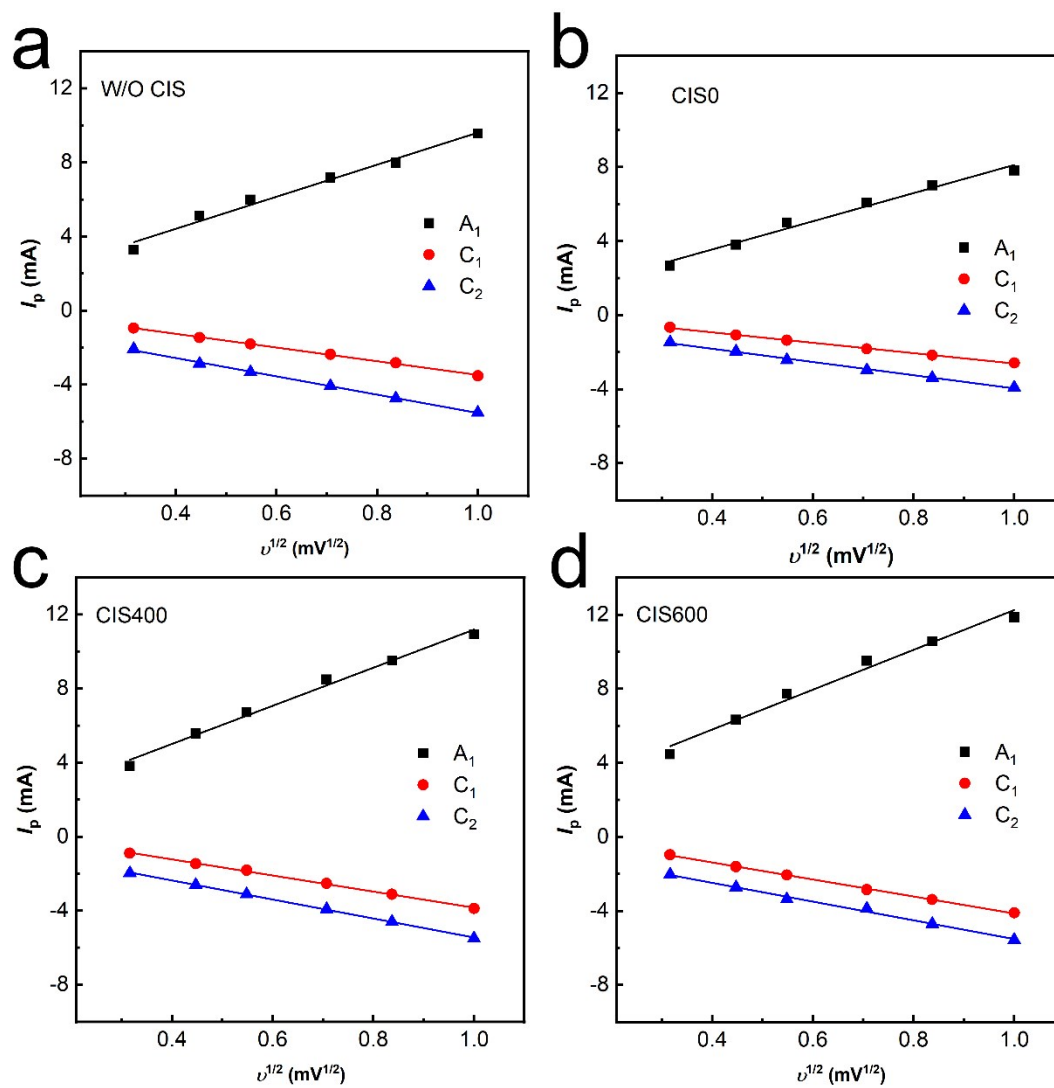


**Fig. S8** The peak intensities of the CV curves obtained at different scan rates for Li-S batteries a) without CIS and with b) CIS0, c) CIS400, d) CIS600.

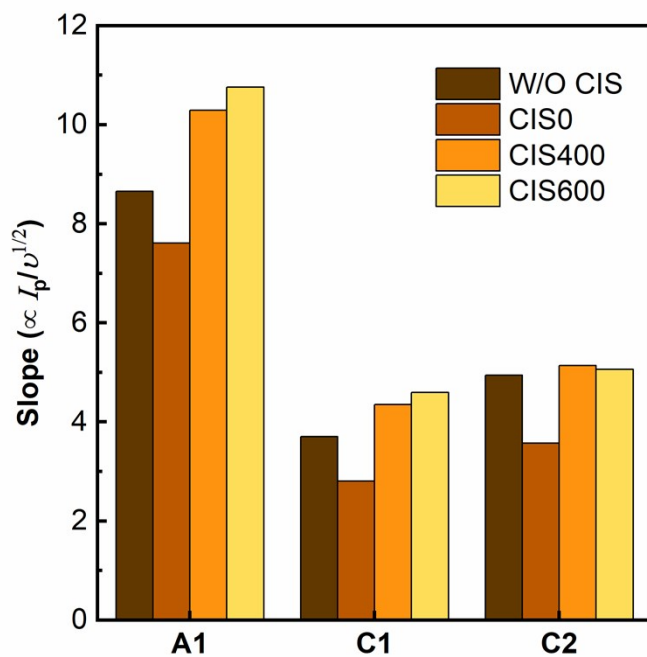


**Fig. S9** The linear fitting slopes from the peak intensities of the Li-S batteries at different CV scan rates.

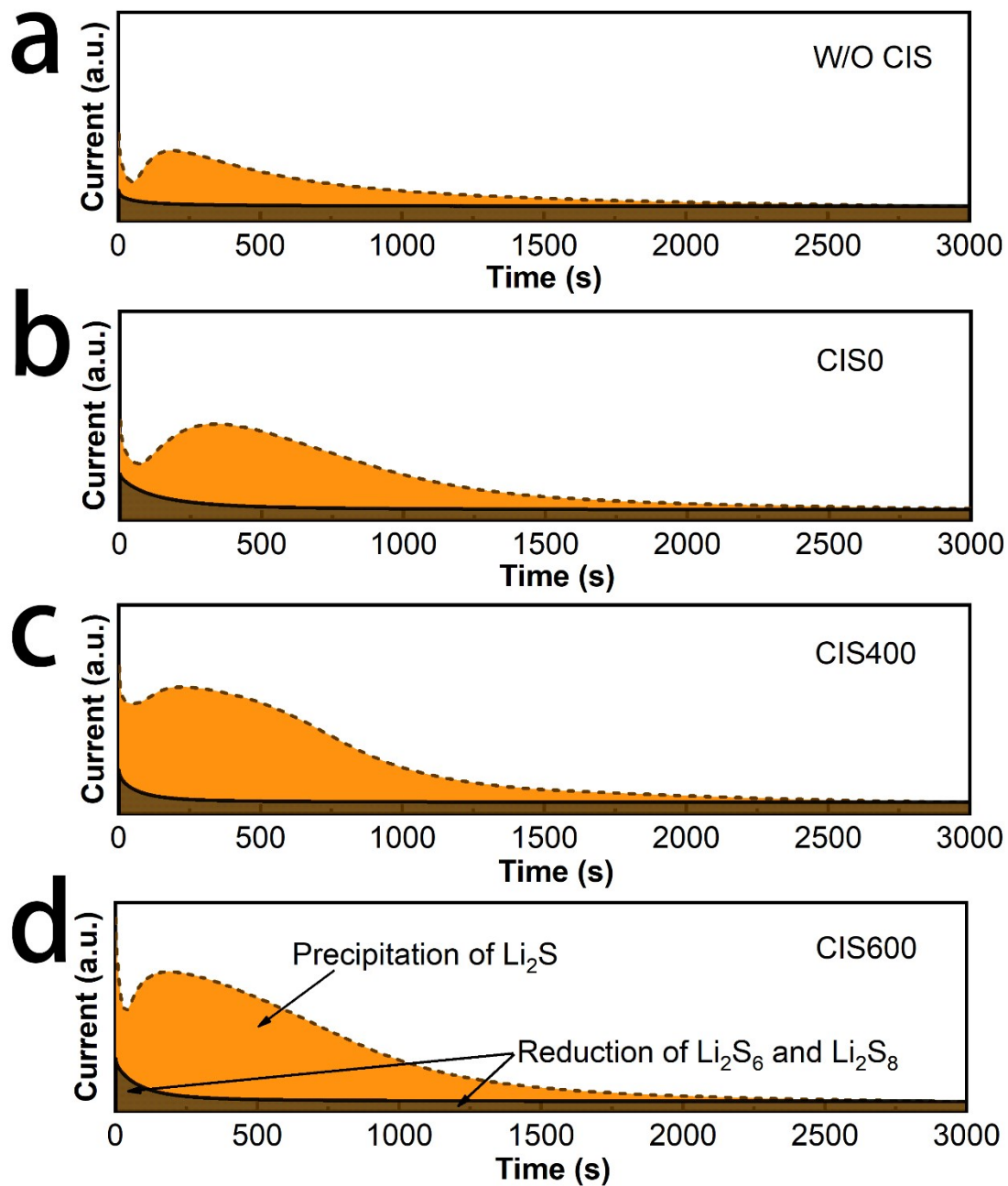


**Fig. S10** Polysulfides deposition profiles. The dark areas represent the reduction of  $\text{Li}_2\text{S}_8$  and  $\text{Li}_2\text{S}_6$ , which are obtained by potential-static discharging at 2.15 V until the current reduces to less than 1% of the initial current. The light areas are assigned to the deposition of  $\text{Li}_2\text{S}$ , which are measured by potential-static discharging at 2.06 V, followed by subtracting the contribution from the reduction of  $\text{Li}_2\text{S}_8$  and  $\text{Li}_2\text{S}_6$ .



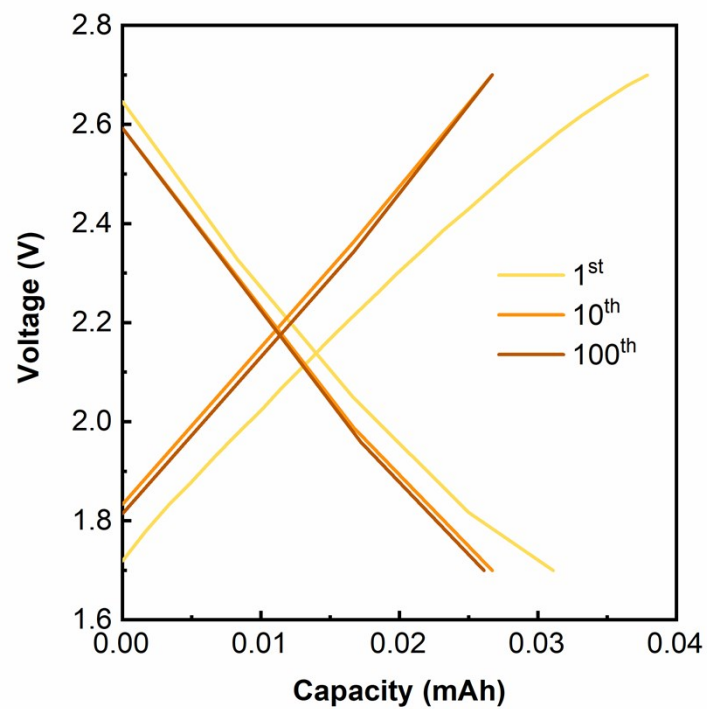


**Fig. S11** Voltage profiles of the battery without sulfur.

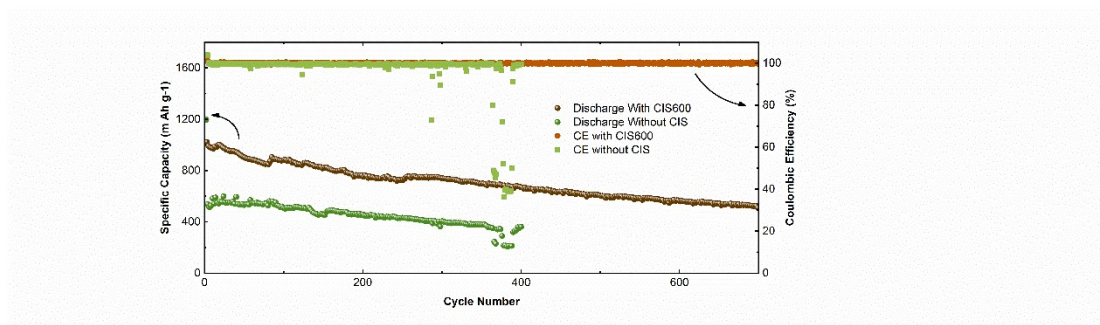


**Fig. S12** Cycling performance of the batteries with and without CIS600.

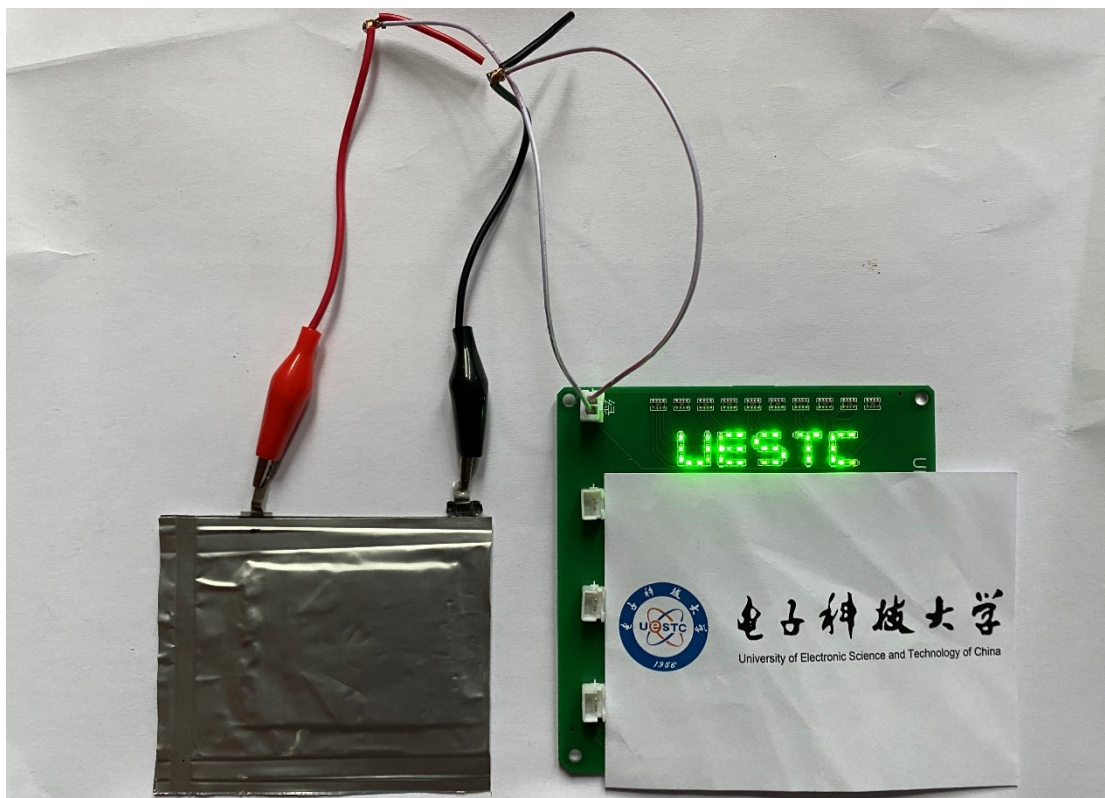


**Fig. S13** Li-S punch cell powering a LED panel.

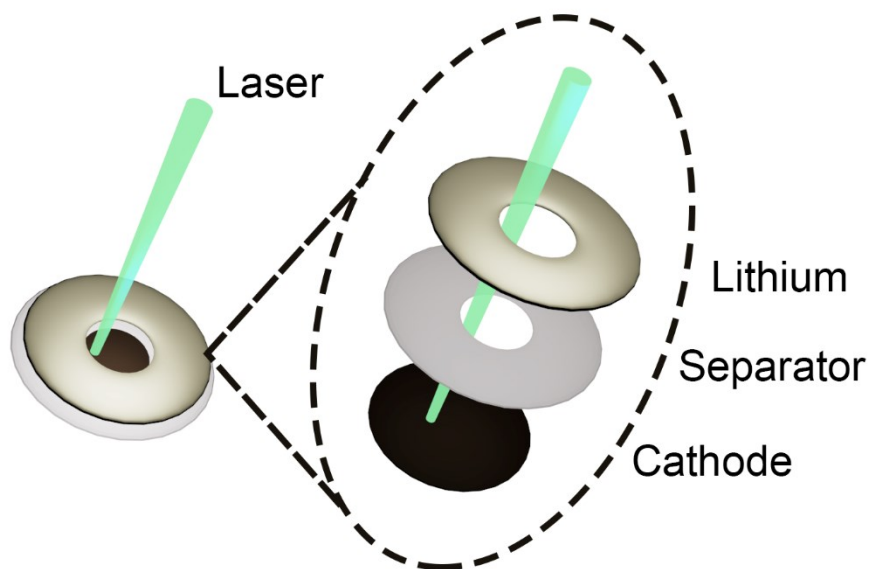


**Fig. S14** Illustration of the in-situ cell configuration.

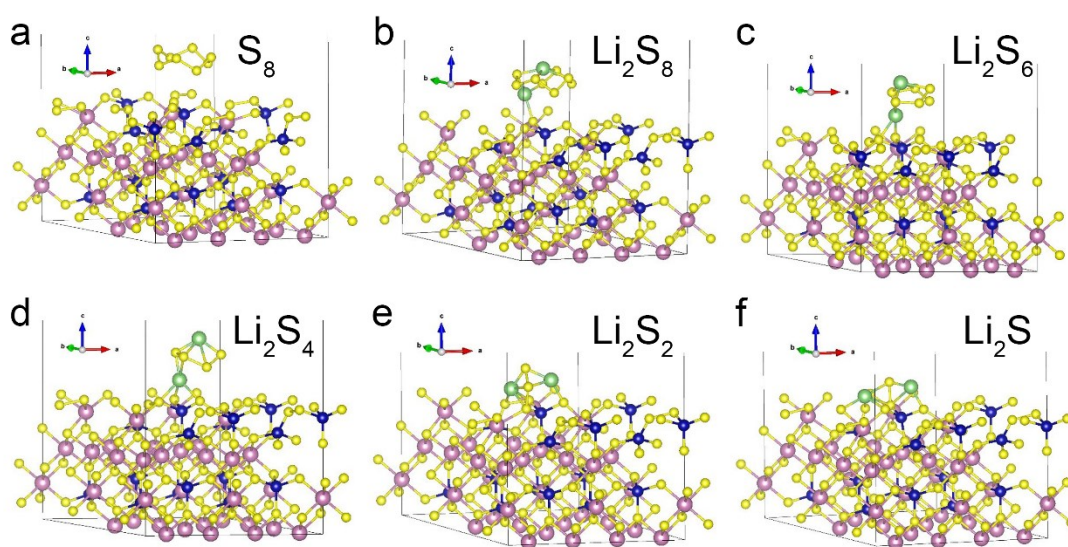


**Fig. S15** Optimized Configurations of LiPSs on the surface of CIS.

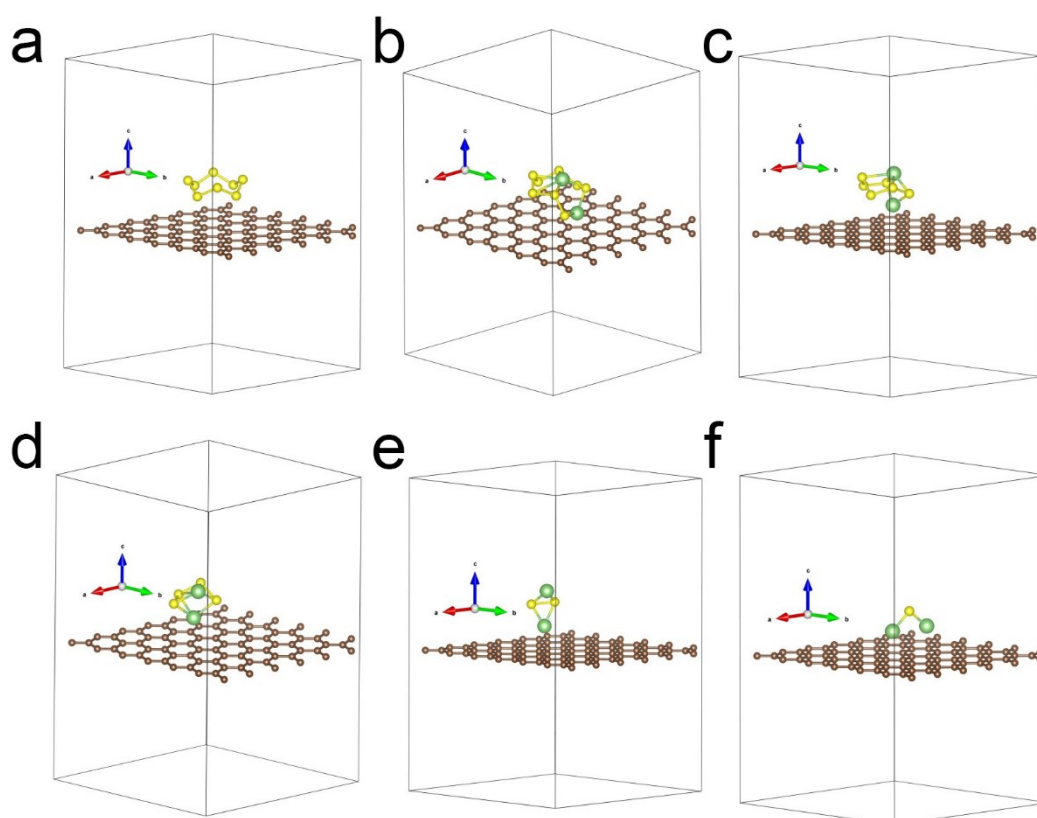


**Fig. S16** The optimized configurations of LiPSs on Graphene.

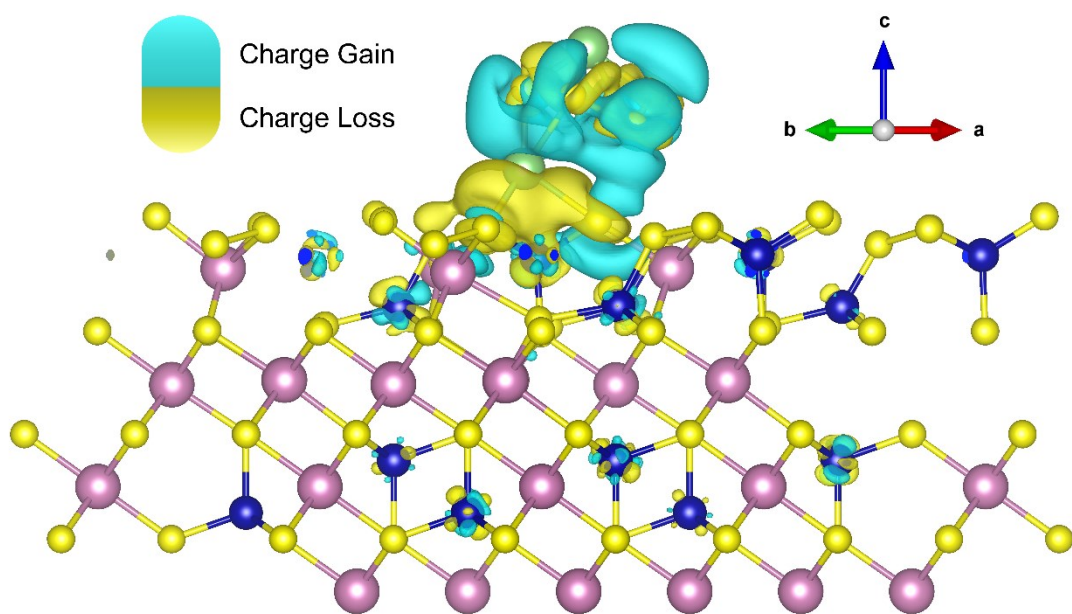


**Fig. S17** Charge density difference analysis of  $\text{Li}_2\text{S}_4$  on CIS considering magnetism.

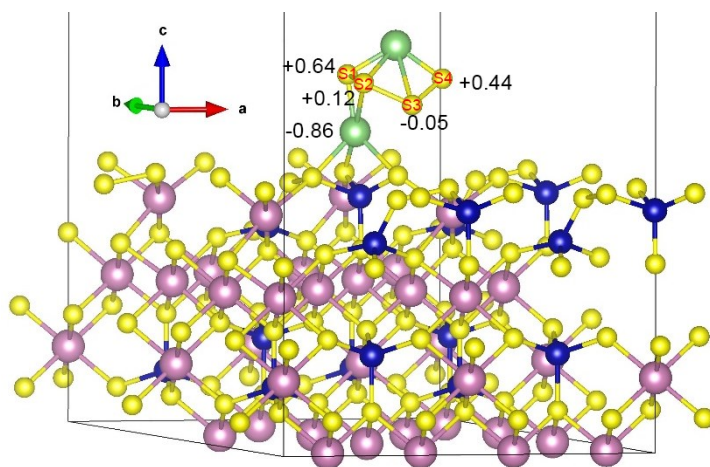


**Fig. S18** Bader charge analysis of  $\text{Li}_2\text{S}_4$  on the surface of CIS.

